Anisotropy of magnetic susceptibility fabrics in syntectonic plutons as tectonic strain markers: the example of the Canso pluton, Meguma Terrane, Nova Scotia

Keith Benn

Ottawa-Carleton Geoscience Centre and Department of Earth Sciences, University of Ottawa, Ottawa, ON K1N6N5, Canada
Email: kbenn@uottawa.ca

ABSTRACT: The anisotropy of magnetic susceptibility (AMS) is widely and routinely used to measure the preferred orientations of Fe-rich minerals in undeformed and weakly deformed granite plutons. The interpretation of the mapped AMS fabrics depends on rock-textural observations, on the map patterns of the fabrics in plutons, and on comparisons of the pluton fabrics to tectonic structures in the country rocks. The AMS may document emplacement-flow related fabrics, but the emplacement fabrics may be reworked or completely overprinted by rather weak tectonic strains of the magma mush or the cooling pluton, especially in syntectonic intrusions. The Late Devonian Canso granite pluton is an excellent example of overprinting of emplacement fabrics by weak tectonic strains. The Canso pluton was emplaced ca. 370 Ma along the boundary between the Meguma and Avalon tectonic terranes, in the northern Appalachian orogen. The AMS was mapped along two traverses that cross the pluton and that are perpendicular to the terrane boundary. Textural evidence suggests the rocks underwent very modest post-full crystallisation strains. The AMS records the dextral transcurrent shearing that occurred on the terrane boundary during emplacement and cooling of the Canso pluton, supporting interpretations that weakly deformed syntectonic granites can be used as indicators of regional bulk kinematics. AMS fabrics in Late Devonian granites of the Meguma Terrane suggest partitioning of the non-coaxial shearing into the terrane bounding fault, with pure-shear dominated deformation further from the fault. Numerical simulations suggest that the kinematics recorded by the fabrics in the Canso pluton was simple-shear, or transpression or transpression with small components of pure shear oriented perpendicular to the bounding shear zone.

KEY WORDS: AMS, Appalachians, granite, strain partitioning, syntectonic, transpression

It is common practice amongst structuralists and granitologists to classify granitic plutons as pre-, syn- and post-tectonic, referring to emplacement prior to, during or following the cessation of orogenic deformation and metamorphism of the country rocks. Such a classification is useful in the practice of putting chronological brackets on tectonic events by isotopic dating of pluton emplacement. Interpretations of pre-, syn- and post-tectonic intrusions are also important in developing pluton emplacement models. Structural interpretations of pre, syn- and post-tectonic emplacement are based on observations of rock textures, the fabric pattern mapped within plutons and comparisons of pluton fabric patterns with the regional-scale structures that record tectonic events.

This present paper presents new data from a syntectonic granite pluton that show tectonic overprinting of magmatic fabrics by small strains related to shearing on a nearby transcurrent terrane boundary. The Canso pluton is a granite of Late Devonian age that was emplaced near the boundary of the Meguma and Avalon terranes, in the Northern Appalachian orogen. The goals of the study are to demonstrate that the fabrics in weakly deformed plutons can provide excellent kinematic indicators of orogenic deformations, and to make the point that the fabrics must be considered in the tectonic context before they can be potentially interpreted to be markers of magma emplacement flow. Numerical simulations are also presented in order to constrain the kinematics of the tectonic overprint of magmatic fabrics in the Canso pluton.

First, interpretations of fabrics in granite plutons are discussed. Then the tectonic setting of the Canso pluton is explained, the new fabric data are presented and the tectonic overprint of the igneous fabrics is argued. The numerical simulations are presented and used to constrain the kinematics along the Meguma–Avalon terrane boundary.

1. Interpreting pluton fabrics

Mineral fabrics in granite plutons can be interpreted in a kinematic framework related to magma dynamics or to regional tectonics (Paterson *et al.* 1998). In the first case, mineral alignments record magma dynamics driven by body forces related to transport and emplacement of the magma, or to convection driven by thermal gradients within the mostly liquid intrusion. The kinematic history recorded by the fabrics can then be interpreted to record buoyancy-driven magma flow (Cruden & Launeau 1994; Tobisch & Cruden 1995) and possibly the mechanics of intrusion. In the second case, the fabric records post-emplacement tectonic deformation of the crystallising magma mush, or of the solidified pluton as it

 doi:10.1017/S1755691009016028

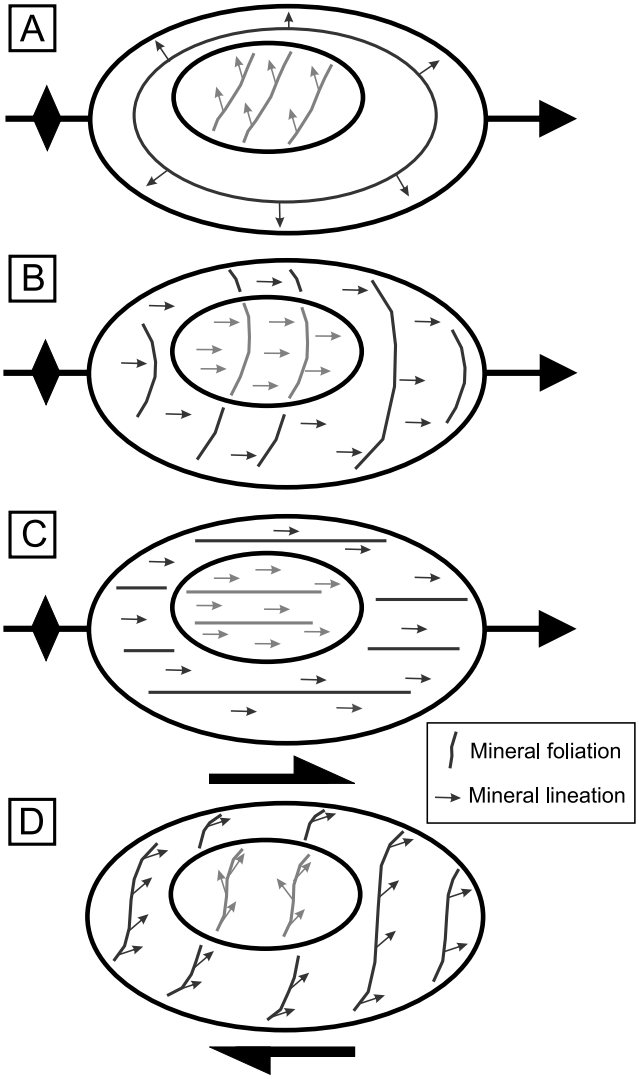

Figure 1 Examples of relationships between fabrics in granite plutons and structures in the country rocks: (A) pluton fabrics are unrelated to country rock structure; (B) probable emplacement-related fabric is folded by regional deformation and lineation is reoriented parallel to the fold hinge; (C) fabric in the pluton is completely overprinted by the regional deformation; (D) pluton emplaced within a region that is undergoing bulk shearing, resulting in partial overprint of the fabric.

cooled from the solidus. The granite fabric then provides information on some (probably small) increment of the regional tectonic strain, and may also be used to infer the tectonic stress field (Benn *et al.* 2001). These two cases are considered to be end-member models. In many published examples of detailed pluton-fabric studies, there is evidence of a partial tectonic overprint of a first generation of mineral alignments that was formed during emplacement flow (Bouchez & Gleizes 1995; Pignotta & Benn 1999; Žák *et al.* 2005; Čečys & Benn 2007).

Figure 1 depicts four examples of fabric patterns in plutons and the relationships of the fabrics to tectonic structures in their host rocks. The precise fabric orientations that are represented in the diagrams are not of primary significance to this discussion. The focus is on the geometric relationships of the fabrics in different nested parts of plutons and on the relationships of pluton fabrics to the tectonic structures. The diagrams in Figure 1 are used to discuss first order interpretations of pluton fabrics. Figure 1A–C depicts plutons emplaced into folded, or folding, country rocks, as indicated by the anticlinal axial surface trace in each figure. Figure 1D shows another example where emplacement occurred during bulk shearing of the host rocks. Cases A and C are similar to pluton fabric development 'completely decoupled' from host rock deformation, and pluton fabric development 'completely coupled' to host rock deformation, as illustrated in figure 13A and C of Paterson *et al.* (1998). Figure 1 includes the necessary analyses of the mineral lineations in plutons which, in practice, are usually determined using the anisotropy of magnetic susceptibility. The interpretation of pluton fabrics is incomplete and risks being erroneous if only the mineral foliations are considered.

In Figure 1A, the pluton fabrics show no geometric relationship to the regional-scale fold. There are also distinct fabric orientations in the nested portions of the pluton that would represent separate magma pulses, indicating the fabrics record the flow kinematics in the two pulses. The structural relationships in Figure 1A suggest that the pluton fabrics record magma flow that was decoupled from deformation in the host rocks, so they can be interpreted to indicate emplacement of the successive magma batches (Vigneresse & Bouchez 1997; Dehls *et al.* 1998; Siegesmund & Becker 2000; Becker *et al.* 2000; Molyneux & Hutton 2000; D'Eramo *et al.* 2006; Razanatseheno *et al.* 2009). This is an example of fabric in a post-tectonic pluton that can be used to infer an emplacement mechanism.

Figure 1 illustrates examples where the fabrics in the plutons are reworked to varying degrees by tectonic deformation. Figure 1B shows a pluton where the foliation is rotated about the regional fold hinge, and the mineral lineation is aligned parallel to the regional hinge. This type of fabric pattern is interpreted to represent folding of a pre-existing foliation in the pluton by regional deformation and reorientation of the lineation parallel to the fold hinge. Figure 1C illustrates a foliation in the pluton that is axial-planar to the regional fold and a lineation that is parallel to the fold hinge. That example represents a stronger tectonic overprint that has resulted in parallelism of the foliation and the lineation in the pluton with the regional structures. Published examples of structural relationships as shown in Figure 1B and C have shown them to indicate emplacement during the regional folding event (Benn *et al.* 1997, 1998; Bolle *et al.* 2003; Čečys & Benn 2007; Pignotta & Benn 1999). The fabrics in the plutons cannot be used to directly infer the kinematics of emplacement flow, or mechanisms involved in pluton emplacement.

In Figure 1D the pluton is emplaced within shearing country rocks. There is an early-formed fabric in the central parts of the pluton that may record magma emplacement flow and it is variably overprinted by the regional shear. The tectonic overprint may begin as the magma in the pluton reaches some threshold of crystallisation, when the solid fraction forms a contiguous framework with increasing strength that transmits anisotropic stresses from the deforming country rocks. Examples like Figure 1D have also been shown to be indicative of syntectonic emplacement (Leblanc *et al.* 1996; Djouadi *et al.* 1997; Gleizes *et al.* 1998; Czeck *et al.* 2006; Gebelin *et al.* 2006).

In examples such as Figure 1B and D, there may be regions of a pluton where igneous textures are preserved; but in no case should the fabrics be interpreted to indicate emplacement flow kinematics, because the fabrics have likely been reworked to some degree by tectonic deformation. The following study serves to illustrate and strengthen the interpretation that, even in granites that would generally be referred to as 'undeformed' or 'weakly deformed', the fabrics may serve as tectonic strain markers.

https://doi.org/10.1017/S1755691009016028 Published online by Cambridge University Press

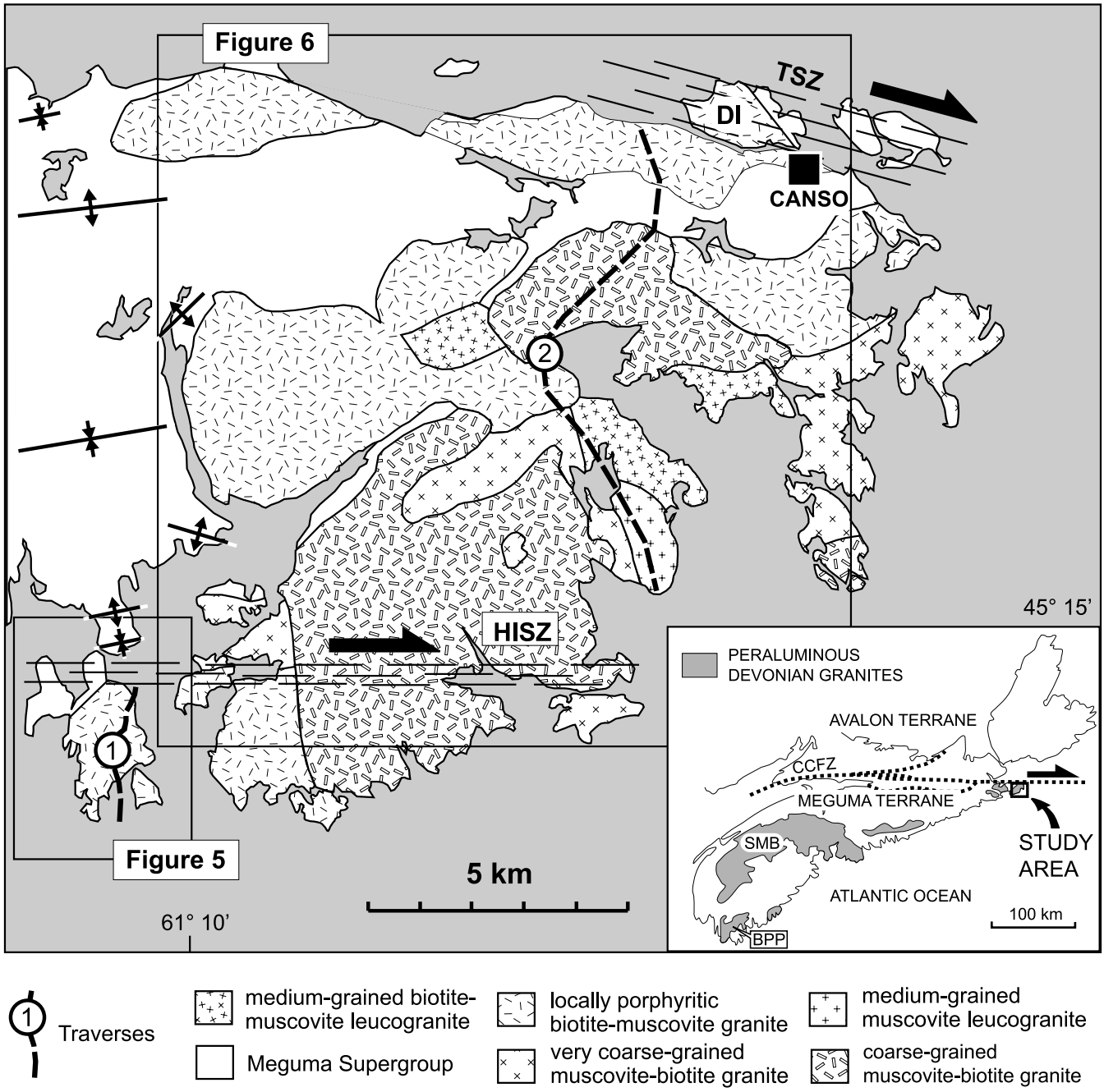

Figure 2 Geological map of the study area, modified from Hill (1991): TSZ, Tittle shear zone; HISZ, Harbour Island shear zone, DI, Durrell's Island. Inset: location map of the Meguma Terrane and the study area: CCFZ, Cobequid–Chedabucto fault zone; SMB, South Mountain batholith; BPP, Barrington Passage pluton.

2. Tectonic setting of the Canso pluton

The Meguma Terrane of southern Nova Scotia (Fig. 2 inset) represents the most internal allochthon recognised within the northern Appalachians (Keppie 1993). The supracrustal rocks are predominantly greenschist to lower amphibolite-grade Cambro-Ordovician metaturbidites of the Meguma Supergroup, which are thought to represent detritus eroded from the Saharan Shield and deposited on the continental slope of northwestern Africa (Schenk 1971, 1995). Collision of the Meguma Terrane with the eastern margin of ancestral North America, represented by the Avalon Terrane (Fig. 2 inset), occurred in the Middle Devonian (Williams & Hatcher 1982; Keppie & Dallmeyer 1987). In Nova Scotia, the boundary between the Meguma and Avalon terranes is represented by the Cobequid–Chedabucto fault zone (CCFZ), which may be linked to a shallowly southward-dipping sole thrust underlying the Meguma Terrane (Keppie 1993). Detailed studies along the CCFZ have revealed a prolonged history of ductile and brittle deformation related to dextral transcurrent tectonics that continued into the Carboniferous (Mawer & White 1987).

The regional structural pattern within the Meguma Supergroup is dominated by upright, shallowly-plunging regional chevron folds (Horne & Culshaw 2001), and associated foliations that trend NNE–SSW in the southern part of the terrane, and that are ENE–WSW trending close to the CCFZ (Keppie 1982). These structures developed during the dextral transcurrent tectonics associated with the Meguma–Avalon collision which is recognised in Nova Scotia as the Acadian Orogeny. Acadian fabric development commenced at about 415 Ma, corresponding to the oldest $^{40}Ar/^{39}Ar$ dates obtained from whole rocks and separates of fabric-forming minerals (Dallmeyer & Keppie 1987; Keppie & Dallmeyer 1987; Muecke *et al.* 1988). $^{40}Ar/^{39}Ar$ dates as young as 360 Ma

https://doi.org/10.1017/S1755691009016028 Published online by Cambridge University Press

Table 1 Characteristics of textural types.

Textural type	Visible fabric	Microstructure
1	None	• Igneous texture preserved • Undulose extinction and subgrains in quartz
2	Weak, vertical foliation defined by quartz aggregates	• Quartz entirely recrystallised into roughly equant new grains, 0·2 to 0·4 mm in size, with highly lobate grain boundaries • Other minerals essentially undeformed
3	Vertical foliation and horizontal extension lineation, both defined by quartz aggregates	• Quartz entirely recrystallised into elongate new grains, $\leq$0·2 mm in size, with straight or gently curved grain boundaries • Mica and feldspars deformed and locally recrystallised

obtained from the Meguma Supergroup (Keppie & Dallmeyer 1987) probably represent thermal resetting during the emplacement of huge volumes of peraluminous granite magma throughout the Meguma Terrane, including the South Mountain batholith (Clarke *et al.* 1993), the Barrington Passage pluton (Reynolds *et al.* 1987) and the Canso pluton, which is the subject of the present study. Geochronological data indicate that the granitic plutons of the Meguma Terrane crystallised between 380 Ma and 365 Ma (Clarke & Halliday 1980; Reynolds *et al.* 1981; Hill 1988; Keppie *et al.* 1993; Tate *et al.* 1997).

Extensive structural, AMS and gravity modelling studies of the large, composite South Mountain batholith showed it to be composed of tabular intrusions, emplaced within a compressional tectonic stress field, resulting in folding of emplacement-related horizontal foliations, and lineations that are parallel to the regional fold axis (Benn *et al.* 1997, 1999). A detailed fabric and AMS study of the Barrington Passage pluton, in the southwestern Meguma Terrane, revealed a similar fabric pattern to the one depicted in Figure 1B (Pignotta & Benn 1999).

3. The Canso pluton and its host rocks

The study area is located along the southern margin of the CCFZ, near the town of Canso, at the eastern tip of the Nova Scotian mainland (Fig. 2). The country rocks are composed of amphibolite-grade psammites and pelites of the Goldenville and Halifax Groups of the Meguma Supergroup. The rocks were strongly deformed during the Acadian Orogeny, resulting in the formation of several generations of vertical, NE–SW to ENE–WSW-trending foliations associated with tight, upright, shallowly plunging folds (Mawer & Williams 1986; Mawer & White 1987). The Canso pluton is discordant to those regional structures, but the contact-parallel folds mapped by Hill (1991) along its western margin (Fig. 2) may record shortening in the wall rocks due to expansion of the pluton during emplacement, as suggested for pluton margin parallel folds near the contact with the South Mountain batholith (Benn *et al.* 1999). Porphyroblasts of biotite, garnet and andalusite include dextrally crenulated segments of the regional foliation within the metamorphic aureole around the pluton, demonstrating emplacement after the development of the regional foliations (Mawer & Williams 1986; Mawer & White 1987; Hill 1991). Two vertical, E–W to WNW–ESE-striking mylonitic shear zones affect the pluton (Fig. 2). Both contain horizontal extension lineations and consistently dextral shear sense indicators (C-S fabrics), showing that the granites were affected by the regional dextral shearing that continued following full crystallisation, and as the pluton cooled.

The Canso pluton was mapped in detail by Hill (1991), who defined the lithological units shown in Figure 2. The granites tend to be homogeneous in both composition and grain size at the outcrop scale. Comagmatic enclaves are rare, and centimetre-scale feldspar phenocrysts are only locally present; therefore the orientations of those markers cannot be mapped systematically. The horizontal two-dimensional nature of most outcrops (except locally along the Atlantic ocean shoreline) also makes field mapping of mineral-preferred orientations difficult. However, shallowly dipping foliations defined by tabular feldspar crystals were reported for a few outcrops of undeformed granites (Hill 1988).

Where autoliths of one magmatic unit are found within another, they tend to be rounded, and the strike of the pre-full crystallisation feldspar foliation is parallel in the autoliths and in the host granite, suggesting that both host and autoliths were deformed together in the magmatic state. This suggests that the different magmatic units in Figure 2 were emplaced contemporaneously, which is consistent with similar monazite crystallisation dates obtained from the different units of 373 Ma to 367 Ma ($^{207}Pb/^{235}U$; T. Krogh *in* Hill 1991). $^{40}Ar/^{39}Ar$ cooling dates obtained for a relatively undeformed sample of granite vary from 366 Ma to 362 Ma (biotite and muscovite separates (Keppie & Dallmeyer 1987)), indicating that the pluton had cooled to about 300°C within $\leq$11 Ma following monazite crystallisation.

4. Rock textures

Microstructures show whether the rock fabric was formed in response to deformation of the crystallising magma, or if some degree of post-full crystallisation overprint may have reworked the magmatic fabric (Paterson *et al.* 1989; Bouchez *et al.* 1990; Vernon 2000). Three microtextural types are defined here for the Canso pluton. The textural types can be correlated with the strength of the mineral fabrics determined in the field, and also using the AMS, and their distinguishing characteristics are given in Table 1.

Rocks of textural type 1 are found at 14 sites, all at distances greater than 1500 m from the mylonitic shear zones. In the field, the rock has no visible fabric, and in thin section there is evidence of only very limited post-full crystallisation strain. The igneous texture is well preserved, and grain-scale ductile strain features are limited to undulose extinction and minor subgrain development in quartz (Fig. 3A).

Closer to the shear zones, there is a transition in the characteristic microstructures, recording an increase in post-full crystallisation deformation. In textural type 2, quartz is recrystallised, though micas and feldspars show little evidence of intracrystalline strain. Quartz new grains are relatively large (Table 1) and have highly lobate grain boundaries (Fig. 3B), suggestive of grain boundary migration, a high temperature recovery mechanism. The new grains form slightly elongate aggregates that define a weak, vertical foliation as observed in the field.

Closer to the shear zones, in rocks of textural type 3, the quartz aggregates are more elongate (defining an easily

https://doi.org/10.1017/S1755691009016028 Published online by Cambridge University Press

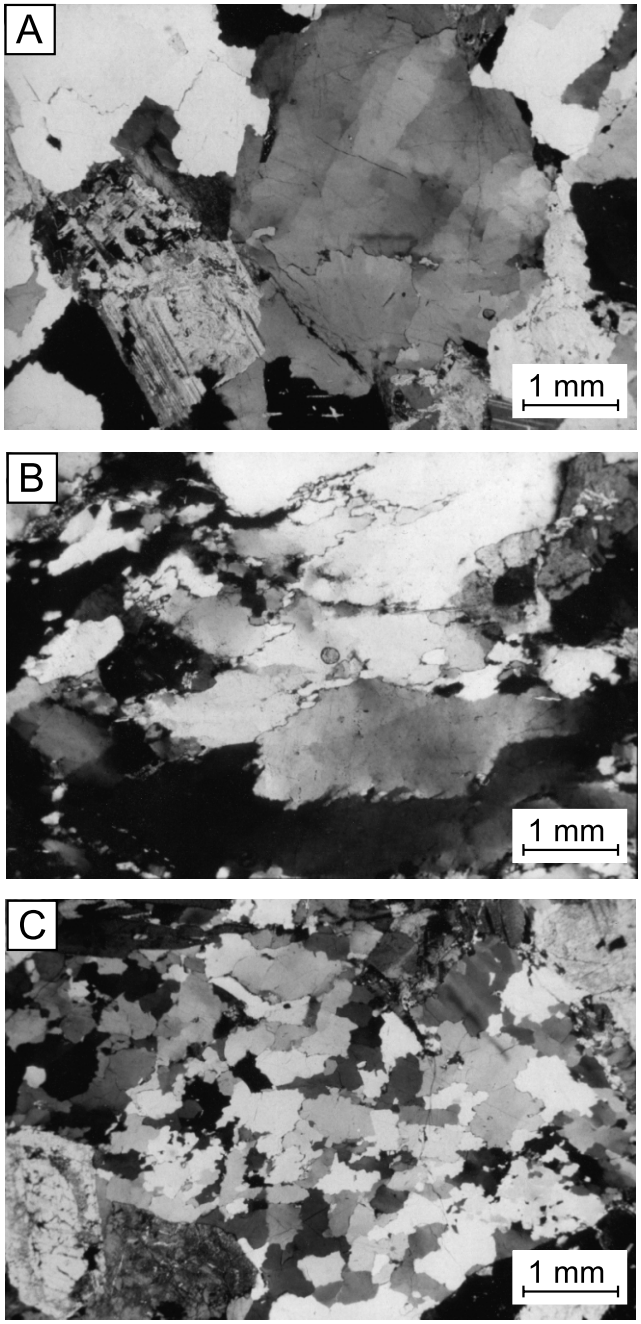

Figure 3 Photomicrographs of the three microstructural types defined in the text: (A) Type 1, from site 19; (B) Type 2, from site 8; (C) Type 3, from site 11.

recognised foliation in the field) and new grains tend to be smaller than in type 2 (compare Fig. 3B and C). The quartz–quartz grain boundaries are lobate, suggesting recrystallisation under fairly high temperature conditions, but the smaller size of quartz new-grains compared to type 2 suggests greater flow stresses (Urai *et al.* 1986) that can be attributed to minor cooling of the pluton during shearing. Some grain-scale shear instabilities (shear bands) are present in type 3 samples which is thought to be indicative of shearing in granites that have cooled to $\approx 500°C$ (Gapais 1989).

The above observations indicate that in rocks of textural type 1, which show no sign of significant subsolidus deformation, the preferred orientations of early formed minerals, such as biotite and euhedral feldspars, will record deformation of the granite magma. On the other hand, the clear imprint of strain and recrystallisation in textural types 2 and 3 shows that fabrics in these rocks have been reworked to some degree, by deformation which occurred after full crystallisation of the magma. The evidence for increasing strain and dynamic recrystallisation under decreasing temperature conditions as the shear zones are approached suggests that fabrics in rocks of textural types 2 and 3 record deformation during subsolidus cooling of the granites, and a progressive localisation of subsolidus strain into the shear zones.

5. Anisotropy of magnetic susceptibility (AMS)

The anisotropy of magnetic susceptibility (AMS) is a method that has proven to be efficient and accurate for measuring the preferred orientations of Fe-minerals in granites, in order to map the fabrics at the pluton-scale (Bouchez 1997, 2000). Sampling for the AMS study was carried out at 30 outcrops along two traverses, mostly following roads and along the Atlantic coastline. No sampling was done for AMS within the mylonitic shear zones, as the fabrics are easily measured in the field, and because the presence of pervasive composite planar fabrics (S-foliation and shear bands) would lead to complex magnetic fabrics (Housen *et al.* 1993; Aranguren *et al.* 1996) that are of no interest in the present study.

Traverse 1 extends from 100 m to 2500 m south of the Harbour Island shear zone (HISZ, Fig. 2), with a maximum spacing between sampling sites of 300 m. Traverse 2 extends from 150 m south of the Tittle shear zone (TSZ, Fig. 2) to 1500 m north of the HISZ, with distances of 125 m to 3000 m between sites. Whereas traverse 1 is entirely within a single intrusive unit of homogeneous muscovite–biotite granite, traverse 2 crosses several internal contacts, and sampling sites therefore represent different intrusive units. Two specimens of 22 mm-length were cut from each of three 25 mm-diameter drill cores collected per sampling site. Thus individual sites are represented by approximately 65 cm^3 of rock. Individual drill cores were separated by several metres in the outcrops in order to obtain a representative sampling.

The AMS was measured at the University of Ottawa using a Kappabridge KLY-2 a.c. bridge (manufactured by AGICO, Czech Republic), in a field strength of 300 A/m at a frequency of 920 Hz. The AMS of each sample is represented by a second order tensor from which the magnitudes of the principal susceptibilities ($K_1 \geq K_2 \geq K_3$), and the orientations of the principal directions (K_n) were obtained. Calculation of site-average AMS tensors and of confidence ellipses about each of the average principal directions was performed using the Hext–Jelinek tensor averaging method (Jelinek 1978, 1981; Borradaile 2003). The confidence ellipses represent the statistical estimates of the areas on the sphere within which 95% of the most probable average orientations of the AMS axes are included.

5.1. Source of the AMS signal

The AMS of a rock sample represents the sum of the intrinsic susceptibility anisotropies of all of the constituent crystals (Hrouda 1982; Borradaile 1988; Rochette *et al.* 1992). The essential minerals of the Canso pluton are biotite+muscovite+plagioclase+K-feldspar+quartz, and accessory minerals include ilmenite, apatite, monazite, garnet and zircon. The mineral assemblage is typical of the ilmenite-series of granites, where titanomagnetite is generally absent (Ishihara 1981; Barbarin 1990). Biotite makes up from 3% to 10% of the rock, and it is the most abundant mineral containing significant amounts of Fe. Its contribution should therefore be predominant in the susceptibility signal of most samples. The susceptibility of ilmenite is greater than that of biotite ($K_{ilmenite} \approx 1$ SI, $K_{biotite} \approx 10^{-3}$ SI; Borradaile 1988), and should this

https://doi.org/10.1017/S1755691009016028 Published online by Cambridge University Press

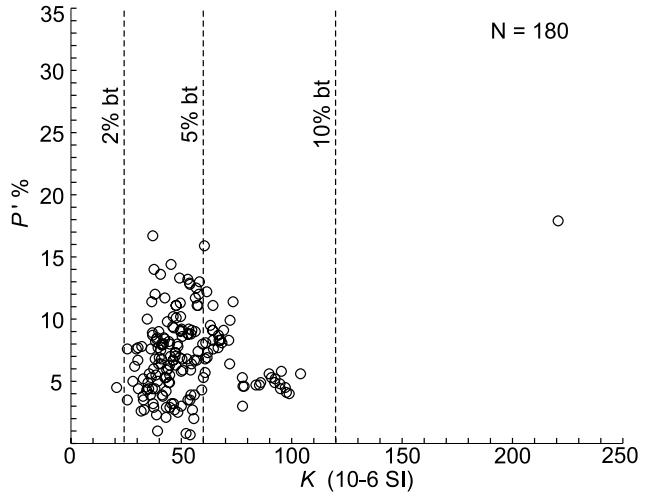

Figure 4 Plot of the degree of magnetic anisotropy (P'%) against the susceptibility (K) for all samples. The dashed lines indicate K values for rocks where the susceptibility is entirely due to 2%, 5%, and 10% biotite, assuming susceptibility $K = 1200 \times 10^{-6}$ SI for biotite.

mineral be locally present in more than trace amounts, it could significantly affect the AMS. We must also consider the presence of very fine grained secondary oxides which may form in association with small amounts of chlorite replacing micas (Benn *et al.* 1993; Borradaile & Werner 1994).

Figure 4 is a plot of the average susceptibility (K) for all samples against P′%=(P′ − 1)*100. P′ is the degree of anisotropy parameter suggested by Jelinek (1981),

$$P' = exp\sqrt{2[(\eta_1 - \eta_m)^2 + (\eta_2 - \eta_m)^2 + (\eta_3 - \eta_m)^2]},$$

where $\eta_i = ln(K_i)$ (i=1 to 3), and $\eta_m = 3\sqrt{\eta_1 \cdot \eta_2 \cdot \eta_3}$. P′% was calculated following the addition of an isotropic diamagnetic (negative) susceptibility component to the measured AMS. The addition of this component is intended to eliminate the effects of the diamagnetic quartz–feldspar matrix in rocks with weak magnetic susceptibility (Rochette 1987; Bouchez *et al.* 1990). The isotropic component $K_{dia} = -6 \times 10^{-6}$ SI corresponds to equal contributions from quartz and feldspar, based on susceptibility data reported in Borradaile (1987).

Significant contributions from locally abundant ilmenite, or secondary magnetite, should result in large variations in K in Figure 4. The susceptibilities in the Canso granites are consistently low, with 178 of 180 samples having $K < 10^{-4}$ SI, corresponding to expected values for rocks where K is entirely due to the presence of <10% biotite (Fig. 4).

Although the magnetic susceptibility of the specimens can be mostly accounted for by the quantities of biotite present in the rocks, this may not be true for the anisotropy of the susceptibility, which can be strongly affected by the presence of even small amounts of secondary magnetite (Rochette *et al.* 1992, 1999; Borradaile & Henry 1997). Such cases can be recognised by locally anomalous fabric orientations.

To a good approximation, the AMS in the Canso granites can be interpreted in terms of the biotite petrofabric. Since K_3 for biotite monocrystals is close to the [001] crystallographic axis, the measured *magnetic foliation* ($\perp K_3$) will be parallel to the average orientation of biotite basal planes, which defines a structural foliation. As $K_1 \cong K_2$ for biotite monocrystals, the measured *magnetic lineation* (K_1) is parallel to the mineral lineation, which is defined by the axis about which the platy biotite crystals are statistically aligned (Bouchez 1997).

5.2. Results

The AMS data, including susceptibilities (K), the degree of anisotropy (P′%), the shape parameter for the average AMS ellipsoids (T, defined in the legend of Table 2), and the orientations of the principal directions for each sampling site, are compiled in Table 2.

Figure 5 presents the AMS orientation data for traverse 1. The strike of the vertical quartz–aggregate foliation, a marker of the weak subsolidus strains that affected some of the sampled granites, is also shown in the orientation diagrams for those outcrops where it is developed (textural types 2 and 3, sites 6–12). Rocks of textural type 1 crop out at the nine sites that are furthest from the HISZ. Site 5 is unique in having an anomalous fabric orientation that is interpreted to indicate a strong magnetic signal from secondary oxides, and it will not be further discussed. At all other sites of textural type 1 (nos. 1–4, 25–28) the orientations of the average principal directions are very consistent. K_{1av} (the magnetic lineation) is horizontal or shallowly plunging, with a NNE–SSW (dominantly) to NE–SW trend, which is consistently oblique in a counterclockwise sense by 50° to 75° to the HISZ. At most of the sites, the K_3 principal direction is well grouped, and K_{3av} plunges steeply, indicating a subhorizontal magnetic foliation.

Approaching the shear zone, in rocks of textural types 2 and 3 the AMS fabrics are rotated in a clockwise sense, and the magnetic foliation steepens progressively. The progressive change in orientations of the fabrics is attributed to the small subsolidus strains that were undergone by the granite at those sites, as indicated by the presence of the vertical quartz–aggregate foliation. It is stressed that the quartz foliation is vertical at all of the sites, but the magnetic (biotite) foliation steepens progressively as the shear zone is approached, and as the solid-state deformation is increased, as shown by the microtextural observations. This is interpreted to indicate that the horizontal foliation that is found in the underformed rocks of textural type 1 was reworked by the solid state deformation associated with dextral shearing, and that the horizontal foliation is completely overprinted with increased strain closer to the shear zone.

On traverse 2 (Fig. 6), the AMS fabric orientations define a pattern similar to the one described for traverse 1. At the sites where the rocks are of textural type 1, K_{3av} is subvertical, indicating horizontal to shallowly-dipping magnetic foliations. K_{1av} is subhorizontal, and trends consistently NE–SW to ENE–WSW. The orientations of K_{1av} are counterclockwise oblique to the HISZ and the TSZ, and it rotates in a clockwise manner in the rocks of textural types 2 and 3 as the TSZ is approached.

The magnetic foliation is horizontal (vertical K_{3av}) at sites 16, 17 and 18, where the vertical quartz foliation is present. The biotite foliation, as indicated by the AMS, is *perpendicular to the vertical quartz aggregate foliation* that represents the superimposed subsolidus strain. This is interpreted to indicate that the subsolidus strain that formed the quartz aggregate foliation was superimposed on a horizontal biotite foliation that likely formed during magmatic deformation. The intensity of the subsolidus strain was apparently insufficient to reorient the biotite foliation at those sites.

5.3. Discussion

Maps of the AMS fabric orientations along two traverses through the Canso granite pluton show that an earlier-formed horizontal biotite fabric in the Canso pluton was reworked and locally overprinted by rather minor amounts of ductile strain as it cooled from the solidus. The ductile strain is certainly related to the well documented dextral shearing along the transcurrent Meguma–Avalon tectonic terrane boundary, the

https://doi.org/10.1017/S1755691009016028 Published online by Cambridge University Press

Table 2 Site average magnetic fabric data.

	Traverse 1						Traverse 2				
		Orientations						Orientations			
Site, Type	K 10^{-6} SI	K_1	K_3	Anisotropy P'%	Shape T	Site, Type	K 10^{-6}	K_1	K_3	Anisotropy P'%	Shape T
1, 1	34·28	199/18	101/25	2·1	0·055	16, 2	55·52	262/02	159/81	9·1	0·088
2, 1	42·02	210/23	315/31	1·7	−0·826	17, 2	62·08	259/04	008/79	7·9	−0·259
3, 1	34·16	019/12	132/63	5·2	0·481	18, 2	50·55	272/12	058/75	11·1	−0·043
4, 1	61·13	046/00	296/89	3·7	−0·037	19, 1	25·10	231/09	102/76	2·4	0·331
5, 1	40·95	323/56	094/24	2·7	0·401	20, 1	33·58	057/04	310/76	4·8	−0·598
6, 2	41·51	218/10	343/73	5·3	−0·565	21, 2	30·09	262/06	170/12	3·4	−0·734
7, 2	37·85	221/11	320/39	5·7	−0·456	22, 1	107·1	230/13	124/48	6·7	0·285
8, 2	37·18	225/01	317/45	5·9	−0·288	23, 1	79·72	241/04	351/79	4·7	−0·240
9, 2	31·69	231/05	323/28	5·6	−0·636	24, 1	84·12	264/09	056/80	4·1	−0·082
10, 2	37·63	243/02	333/01	7·1	0·052	25, 1	34·53	195/04	293/66	6·4	0·440
11, 3	36·77	066/05	157/06	9·4	0·261	26, 1	41·66	254/13	035/74	3·2	0·818
12, 3	40·01	071/03	161/01	10·2	0·071	27, 1	45·51	208/07	034/83	2·0	0·250
13, 2	55·58	088/08	352/37	5·8	−0·169	28, 1	36·43	217/05	315/54	5·4	0·119
14, 2	46·42	091/02	000/14	7·4	0·176	29, 3	48·82	092/13	353/34	7·6	−0·771
15, 2	61·79	263/08	166/43	7·4	−0·025	30, 2	52·21	074/01	164/02	6·7	0·190

Site=sampling site; Type=Textural type (see Table 1); K=magnetic susceptibility; K_1, K_3=principal directions of the anisotropy of magnetic susceptibility; P'%=degree of anisotropy *100 (see text); $T=2(\ln K_2 - \ln K_3/(\ln K_1 - \ln K_3) - 1$ describes the shape of the AMS ellipsoid (Jelinek 1981), where $T=1$ for a perfectly oblate ellipsoid, and $T=-1$ for a perfectly prolate ellipsoid.

CCFZ. The dextral-shear overprint of the fabrics in the Canso pluton confirms that dextral displacements occurred on the CCFZ at 370 Ma. The results also support the use of fabrics in weakly deformed granites to determine the bulk kinematics in orogenic belts, as previously proposed for leucogranites of the Pyrenées mountain belt (Leblanc *et al.* 1996; Gleizes *et al.* 1997).

Previous magnetic fabric studies of the South Mountain batholith (Benn *et al.* 1997) and of the Barrington Passage pluton (Pignotta & Benn 1999), both of which crop out within the Meguma Terrane but far from the transcurrent Meguma–Avalon terrane boundary, showed that the magnetic lineations in the plutons were reworked into orientations parallel to the regional fold axes. In the Canso pluton, which crops out quite close to the transcurrent terrane boundary, the lineations are not parallel to the regional fold hinges; instead, they are oblique to the terrane-bounding shear zone. It is proposed that this difference in the fabric record can be attributed to strain and displacement partitioning in a bulk transpressional orogen (Tikoff & Teyssier 1994). In the South Mountain batholith and the Barrington Passage plutons, the fold-parallel fabrics are indicative of bulk pure shear in the folded rocks far from the terrane bounding shear zone, whereas the fabrics of the Canso pluton record the partitioning of orogen-parallel displacements and bulk non-coaxial strains into the CCFZ.

Another point can be made that is of interest for interpretations of AMS fabrics in granites, in general. The fabrics in the rocks of textural type 2 have certainly been reworked by a weak tectonic strain, resulting in the reorientation of the lineations and a steepening of the foliation. In those rocks the evidence of solid-state strain is limited to the elongation of recrystallised quartz aggregates, whereas feldspar and mica crystals are for the most part undeformed. Therefore, it should be noted that the fabrics in such weakly deformed rocks cannot be easily interpreted as recording only magmatic deformation or emplacement-related strain.

For example, on traverse 1, the AMS measurements of samples from several sites of textural type 1 reveal horizontal foliations and magnetic lineations that are oriented NNE–SSW, making angles as great as 75° with respect to the HISZ. Those fabrics might be interpreted as indicating a horizontal NNE–SSW flow during emplacement of the granitic magma, with the flow trajectory oriented perpendicular to a feeder zone represented by the nearby CCFZ, in a manner similar to the interpretation of magnetic anisotropy fabrics in the Archean Lebel syenite pluton, Canada (Cruden & Launeau 1994). However, given the tectonic overprint of fabrics elsewhere in the Canso pluton, it is stressed that interpretations of the AMS in terms of magma emplacement, in this study, would be highly equivocal.

6. Fabric overprinting in transpression

This section investigates the possibility of constraining the kinematics of the non-coaxial strain that was partitioned into the transurrent terrane boundary during advanced stages of collision of the Meguma and Avalon terranes. A recent study of syntectonic granites in the Vosges Mountains of France proved successful in modelling AMS fabric development and strain partitioning in an overall transtensional regime (Kratinova *et al.* 2007). A slightly different approach to the numerical simulations is taken to the one used by those authors, but the aim of the modelling is similar.

Numerical models can been applied to predict the evolutions of petrofabrics of populations of mineral grains during progressive strain histories, and the modelled petrofabrics can then be used to easily calculate the expected AMS, which can be compared to the measured AMS of rocks to infer strains and strain paths (Richter 1992; Hrouda 1993). The approach used here is similar to that used by Benn 1994, but the progressive strain is transpressional, rather than simple shear and pure shear.

The preferred orientation of the c-axes of biotite crystals was measured for a sample from site CN3 (traverse 1), using a universal stage. Site CN3 is classified as textural type 1, and the AMS indicated a horizontal biotite foliation and a NNE–SSW lineation (Fig. 5). The measured biotite fabric was subjected to successive small strain increments, using the incremental strain matrix,

https://doi.org/10.1017/S1755691009016028 Published online by Cambridge University Press

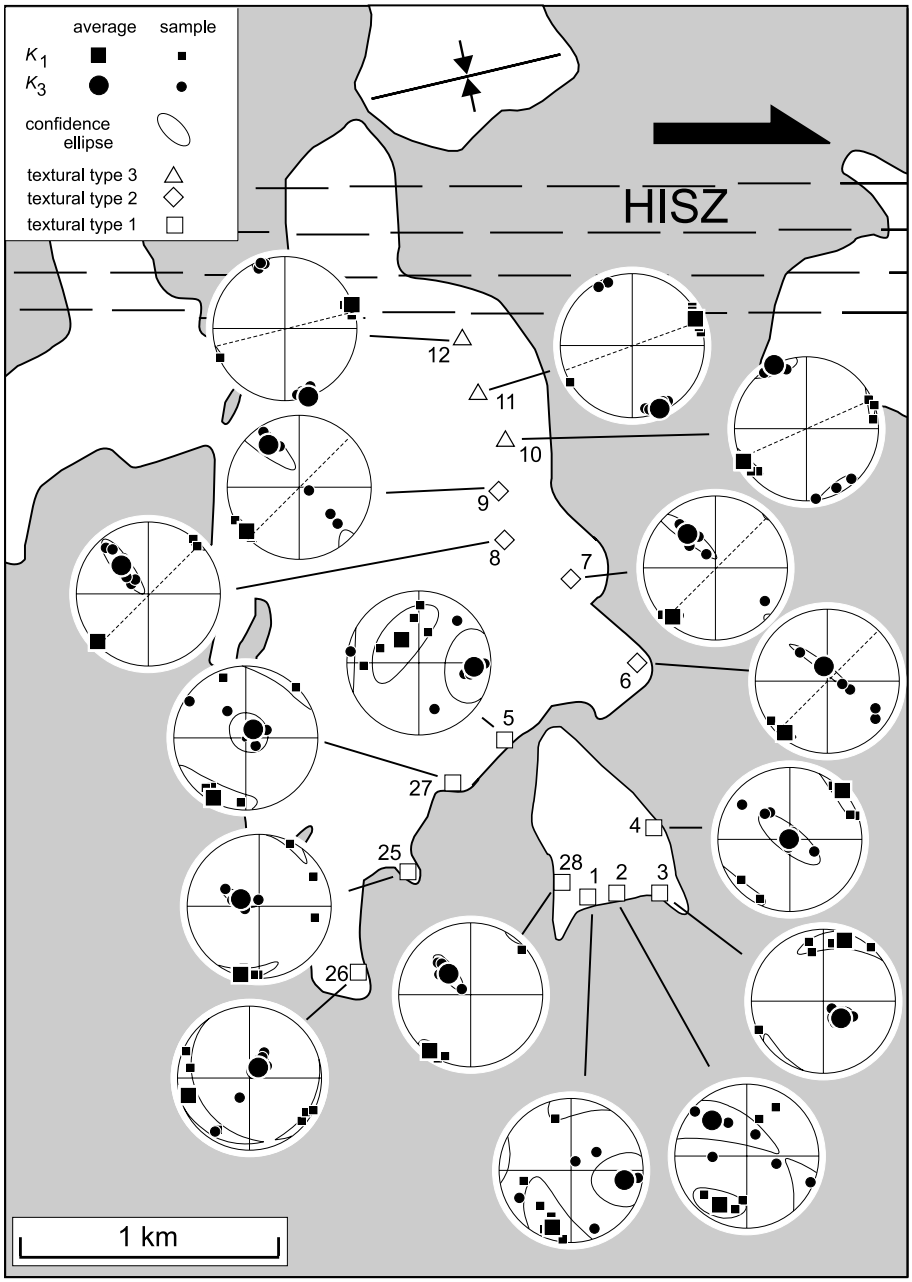

Figure 5 Map of traverse 1, south of the Harbour Island shear zone (HISZ). The number of each sampling site is indicated next to the site. The principal directions of the AMS are shown in lower-hemisphere equal-area projections. Dashed lines in some projections indicate the trace of the vertical quartz–aggregate foliation measured in outcrop. The map area is located in Figure 1.

$$\begin{bmatrix} a & -\gamma & 0 \\ 0 & 1 & 0 \\ 0 & 0 & a^{-1} \end{bmatrix}$$

to simulate progressive, homogeneous strain of the biotite c-axis petrofabric. This is the kinematic model of transpression proposed by Sanderson & Marchini (1984). The dextral simple-shear component of strain takes place along vertical east–west planes, parallel to the CCFZ. γ represents the incremental shear strain. a^{-1} represents the incremental stretch of a line oriented north–south horizontal, and a represents the incremental stretch of a vertical line.

The parameter $T_i=\gamma_i(1-a_i^{-1})^{-1}$ is used to indicate the relative contributions of incremental pure shear and incremental simple shear (Sanderson & Marchini 1984). Positive values of T_i indicate 'transpression', in the sense that the pure shear component of incremental strain has a vertical X-axis and a horizontal, N–S oriented Z-axis. Negative values of T_i indicate 'transtension', where the pure shear component of incremental strain has the Z-axis vertical and the X-axis N–S horizontal. $|T_i|\rightarrow 0$ indicates an increasing component of incremental pure shear and $T_i=\infty$ indicates simple shear. The incremental strains were calculated with γ held constant at 0·01, and incremental $a^1=1-(\gamma/T_i)$. At each increment in the strain history, the AMS is calculated by summing the susceptibility tensor for each biotite crystal in the petrofabric population, assuming a perfectly oblate AMS for each crystal and an anistropy value (P′) of 1·35 (Hrouda 1993).

One limitation of the approach is that the shapes of biotite crystals are not taken into account; rotations of crystals are governed by the application of the transpressional strain tensor to the vectors defining the orientations of the c-axes of the

https://doi.org/10.1017/S1755691009016028 Published online by Cambridge University Press

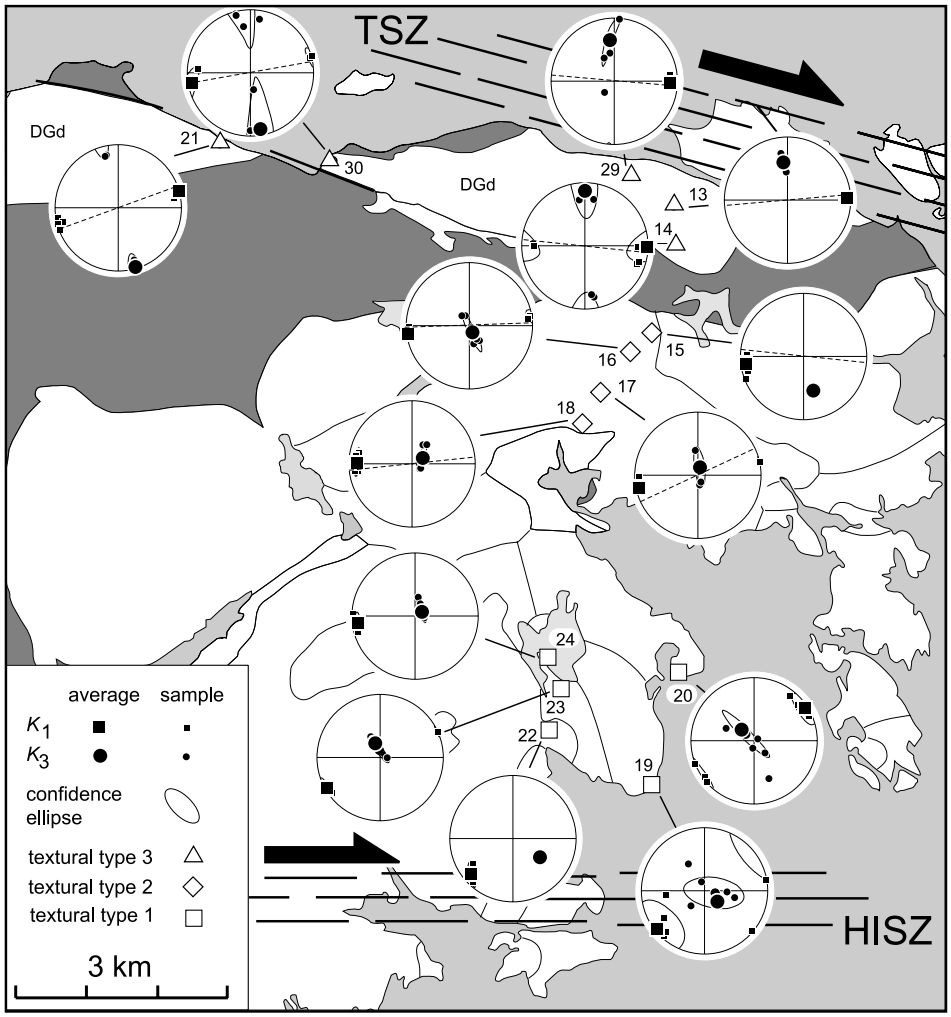

Figure 6 Map of traverse 2, south of the Tittle shear zone (TSZ). The number of each sampling site is indicated next to the site. The principal directions of the AMS are shown in lower-hemisphere equal-area projections. Dashed lines in some projections indicate the trace of the vertical quartz–aggregate foliation measured in outcrop. The map area is located in Figure 1.

crystals. In other words, the biotite crystals are assumed to behave as planes that are reoriented in response to the imposed strain (March 1931). That simplification is not unreasonable for biotite platelets with high aspect ratios. Only small strains are considered here, so that the possibility of periodic petrofabric evolutions which may arise at high strains for populations of crystals with lower aspect ratios (Ildefonse *et al.* 1997) does not need to be taken into account.

The modelling is intended to simulate the variations in the biotite fabric orientations and intensities documented using the AMS, from the undeformed granites of textural type 1 far from the shear zones, through textural types 2 and 3 as the shear zones are approached. An underlying assumption is that the changes in the biotite fabrics along a traverse from type 1 through type 3 represents a time- and strain-progressive overprint of the magmatic fabric at sampling site 3. In support of that interpretation it is noted that strain increases with decreasing distance from the shear zones, as indicated by the intensity of the visible fabric. Also, the microstructures suggest that deformation and dynamic recrystallisation proceeded at slightly lower temperatures as the pluton cooled.

Lower-hemisphere projections of several steps in the progressive evolutions of the strain ellipsoids (modelled extension lineations and foliation poles, Fig. 7A–F) and of the K_1 and K_3 principal directions of the AMS (the magnetic lineation and the pole to the magnetic foliation, Fig. 7G–L) are presented for different strain histories (transpression, transtension and simple shear). The plots show results for steps labelled 1–4, corresponding to strain intensity values of 0·25, 0·50, 1·00, and 1·50. Strain intensities are calculated as (Nadai 1963):

$$\bar{\varepsilon}_s = \sqrt{3}/3[(\varepsilon_1 - \varepsilon_2)^2 + (\varepsilon_2 - \varepsilon_3)^2 + (\varepsilon_3 - \varepsilon_1)^2]^{0.5}$$

For large degrees of incremental N–S shortening, perpendicular to the terrane boundary (transpression, $T_i = 3$, Fig. 7D), there may be a transient stage (steps 2 to 3) where the magnetic fabric path is similar to the pattern mapped in the granites, but at higher strains the magnetic lineation migrates to steeper plunges (steps 3 to 4). The modelled stretching lineation would also be vertical at relatively low strains, as previously shown by Sanderson & Marchini (1984). For large incremental stretches perpendicular to the Minas fault zone (transtension, $T_i = -3$, Fig. 7F), the magnetic foliation would not become vertical and such a strain path could not be responsible for the fabric pattern in the Canso granites.

Progressive simple-shear ($T_i = \infty$, Fig. 7A) and progressive transpressional or transtensional strain histories with small to moderate degrees of incremental pure-shear ($5 \leq T_i \leq 10$, Fig. 7B, C; $T_i = -6$, Fig. 7E) all produce evolutions in the orientations of the strain axes and of the magnetic fabric axes which resemble those mapped across the strain gradients from textural type 1 to textural type 3. In each of these examples the magnetic lineation is oriented close to the stretching lineation at $\bar{\varepsilon}_s \leq 0{\cdot}45$. The magnetic foliation becomes vertical at strain

https://doi.org/10.1017/S1755691009016028 Published online by Cambridge University Press

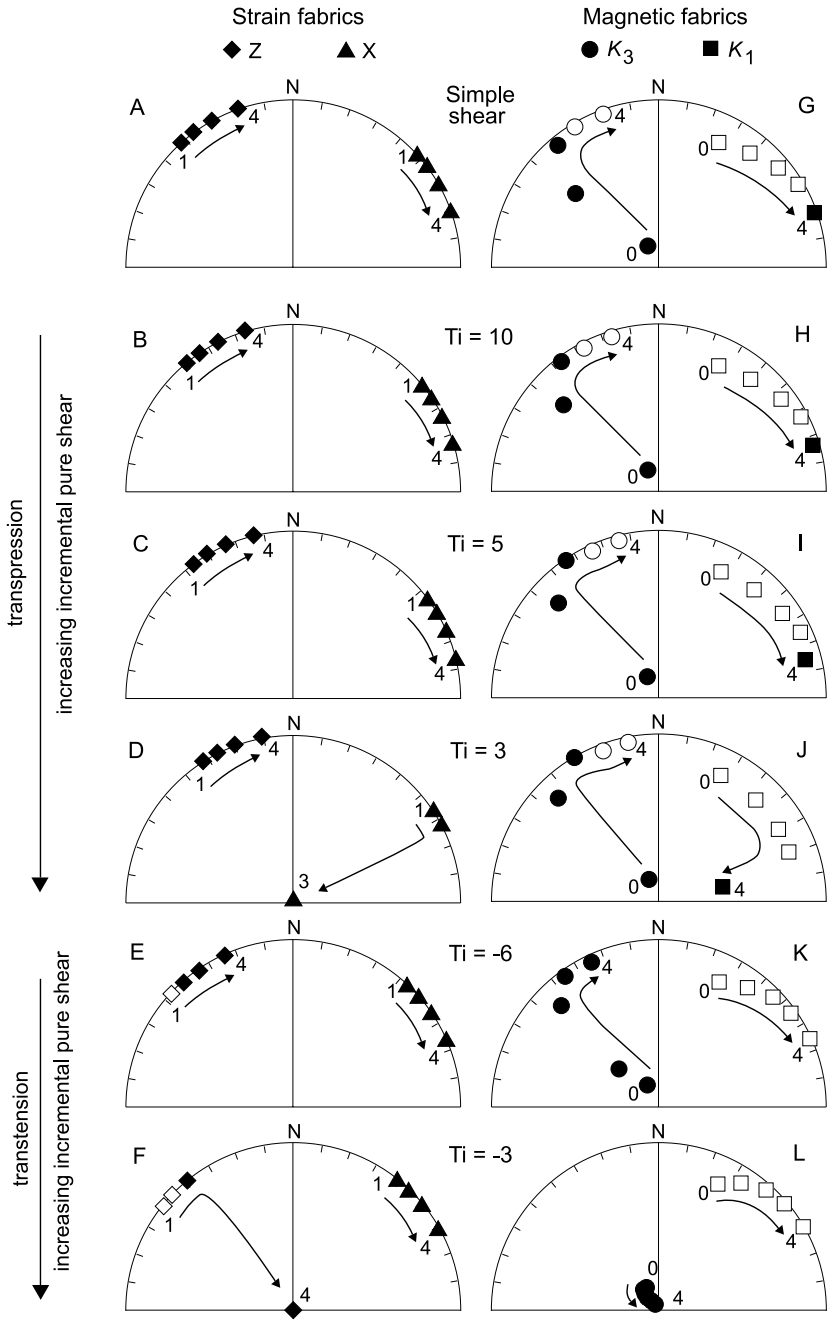

Figure 7 Results of numerical simulations of strain and fabric development during transpression and transtension. The progressive strain histories were applied to an initial biotite petrofabric that was measured for an undeformed granite sample from sample site CN3 (Fig. 5). Equal-area projections. Filled symbols are on the lower hemisphere and open symbols are on the upper hemisphere. Data are plotted for four stages of each strain history. In the magnetic fabrics diagrams, stage 0 is the AMS calculated for the initial petrofabric from sample site CN3.

intensities that are lower during progressive transpressional or simple-shear strain histories than during progressive transtensional strain histories. This is seen by comparing the data for steps 2, $T_i = \infty$, 10 and 5, with that for step 3, $T_i = -6$ (Fig. 7A, B, C and E; Table 2). Increasing progressive transtensional strain could result in verticalisation of the magnetic foliation and in coaxial magnetic and finite strain axes, as seen in more strongly deformed rocks near to the shear-zones (Fig. 7E).

The results of the models presented here suggest that the fabric pattern in the Canso granites could be explained by a progressive strain history represented by simple-shear, or by transpression or transtension with small to moderate components of incremental shortening or stretching perpendicular to the Minas fault zone. The model results indicate that a transtensional strain history would be most likely to preserve the early-formed horizontal magnetic foliation mapped in the rocks of textural type 2, where the magnetic lineation would have rotated to lie in the plane of the mesoscopic quartz-aggregate foliation observed in the field.

7. Conclusions

The anisotropy of magnetic susceptibility (AMS) was used to map the preferred orientations of biotite crystals in a granite pluton that was emplaced during the Late Devonian Acadian Orogeny, in Nova Scotia. The pluton was emplaced near the transcurrent boundary between the Meguma and Avalon tectonic terranes. Careful consideration of the magnetic fabrics in a framework including structural, microstructural and regional tectonic information shows that the AMS fabrics

https://doi.org/10.1017/S1755691009016028 Published online by Cambridge University Press

(inferred to indicate biotite fabrics) preserve a record of syn- to post-emplacement dextral shear on the terrane boundary. The post-emplacement shearing occurred as the pluton cooled from the solidus. An early-formed horizontal fabric, preserved at some sampling sites, was reworked and overprinted by small amounts of tectonic deformation. The results confirm the usefulness of AMS fabrics in weakly deformed syntectonic plutons as markers of the bulk kinematics of orogens. Comparison of the fabrics in the Canso plutons, documented here, with previous results from plutons of similar ages but further from the terrane boundary, within the Meguma Terrane, shows that the fabrics in granites situated within different parts of an orogen can be used to map the partitioning of coaxial and non-coaxial strains that are predicted for transpressional orogens.

Numerical simulations of the fabric evolutions in the Canso pluton suggest that the kinematics of transcurrent shearing along this part of the Meguma–Avalon terrane boundary involved simple-shear or transpression, or transpression with small components of pure shear oriented perpendicular to the bounding shear zone. A markedly transpressional or transtensional progressive strain history is apparently ruled out in this study.

8. Acknowledgements

The field work for this study was funded by a Natural Sciences and Engineering Research Council of Canada (NSERC) research grant to the author. G. S. Pignotta and S. Siegesmund provided reviews that improved the paper.

9. References

Aranguren, A., Cuevas, J. & Tubía, J. M. 1996. Composite magnetic fabrics from S–C mylonites. *Journal of Structural Geology* **18**, 863–9.

Barbarin, B. 1990. Granitoids: main petrogenetic classifications in relation to origin and tectonic setting. *Geological Journal* **25**, 227–38.

Becker, J. K., Siegesmund, S. & Jelsma, H. A. 2000. The Chinamora batholith, Zimbabwe: structure and emplacement-related magnetic fabric. *Journal of Structural Geology* **22** (11–12), 1837–53.

Benn, K. 1994. Overprinting of magnetic fabrics in granites by small strains: numerical modelling. *Tectonophysics* **233**, 153–62.

Benn, K., Rochette, P., Bouchez, J.-L. & Hattori, K. 1993. Magnetic susceptibility, magnetic mineralogy and magnetic fabrics in a late Archean granitoid-gneiss belt. *Precambrian Research* **63**, 59–81.

Benn, K., Horne, R. J., Kontak, D. J., Pignotta, G. & Evans, N. G. 1997. Syn-Acadian emplacement model for the South Mountain Batholith, Meguma Terrane, Nova Scotia: Magnetic fabric and structural analyses. *Geological Society of America Bulletin* **109**, 1279–93.

Benn, K., Ham, N. M., Pignotta, G. S. & Bleeker, W. 1998. Emplacement and Deformation of Granites During Transpression – Magnetic Fabrics of the Archean Sparrow Pluton, Slave Province, Canada. *Journal of Structural Geology* **20** (9–10), 1247–59.

Benn, K., Roest, W. R., Rochette, P., Evans, N. G. & Pignotta, G. S. 1999. Geophysical and structural signatures of syntectonic batholith construction: the South Mountain Batholith, Meguma Terrane, Nova Scotia. *Geophysical Journal International* **136**, 144–58.

Benn, K., Paterson, S. R., Lund, S. P., Pignotta, G. S. & Kruse, S. 2001. Magmatic fabrics in batholiths as markers of regional strains and plate kinematics: example of the Cretaceous Mt. Stuart batholith. *Physics and Chemistry of the Earth* **26** (4–5), 343–54.

Bolle, O., Diot, H. & Trindade, R. I. F. 2003. Magnetic fabrics in the Holum granite (Vest-Agder, southernmost Norway): implications for the late evolution of the Sveconorwegian (Grenvillian) orogen of SW Scandinavia. *Precambrian Research* **121** (3–4), 221–49.

Borradaile, G. 1987. Anisotropy of magnetic susceptibility: rock composition versus strain. *Tectonophysics* **138**, 327–9.

Borradaile, G. J. 1988. Magnetic susceptibility, petrofabrics and strain. *Tectonophysics* **156**, 1–20.

Borradaile, G. J. 2003. *Statistics of Earth Science data.* New York: Springer-Verlag. 351 pp.

Borradaile, G. J. & Henry, B. 1997. Tectonic applications of magnetic susceptibility and its anisotropy. *Earth-Science Reviews* **42**, 49–93.

Borradaile, G. J. & Werner, T. 1994. Magnetic anisotropy of some phyllosilicates. *Tectonophysics* **235**, 223–48.

Bouchez, J.-L. 1997. Granite is never isotropic: an introduction to AMS studies of granitic rocks. *In* Bouchez, J.-L., Hutton, D. H. W. & Stephens, W. E. (eds) *Granite: from segregation of melt to emplacement fabrics*, 95–112. Dordrecht: Kluwer Academic Publishers.

Bouchez, J.-L. 2000. Anisotropie de susceptibilité magnétique et fabrique des granites. *Comptes Rendus à l'Académie des Sciences de Paris, Sciences de la Terre et des planètes* **330**, 1–14.

Bouchez, J.-L., Gleizes, G., Djouadi, T. & Rochette, P. 1990. Microstructure and magnetic susceptibility applied to emplacement kinematics of granites: the example of the Foix pluton (French Pyrenees). *Tectonophysics* **184**, 157–71.

Bouchez, J.-L. & Gleizes, G. 1995. Two-stage deformation of the Mont-Louis-Andorra granite pluton (Variscan Pyrenees) inferred from magnetic susceptibility anisotropy. *Journal of the Geological Society, London* **152**, 669–79.

Čečys, A. & Benn, K. 2007. Emplacement and deformation of the ca. 1.45 Ga Karlshamn granitoid pluton, southwestern Sweden, during ENE–WSW Danopolonian shortening. *International Journal of Earth Sciences* **96**, 397–414.

Clarke, D. B., Chatterjee, A. K. & Giles, P. S. 1993. Petrochemistry, tectonic history, and Sr–Nd systematics of the Liscomb Complex, Meguma Lithotectonic Zone, Nova Scotia. *Canadian Journal of Earth Sciences* **30**, 449–64.

Clarke, D. B. & Halliday, A. N. 1980. Strontium isotope geology of the South Mountain Batholith, Nova Scotia. *Geochimica et Cosmochimica Acta* **44**, 1045–58.

Cruden, A. R. & Launeau, P. 1994. Structure, magnetic fabric and emplacement of the Archean Lebel Stock, SW Abitibi Greenstone Belt. *Journal of Structural Geology* **16**, 677–91.

Czeck, D. M., Maes, S. M., Sturm, C. L. & Fein, E. M. 2006. Assessment of the relationship between emplacement of the Algoman plutons and regional deformation in the Rainy Lake region, Ontario. *Canadian Journal of Earth Sciences* **43** (11), 1653–71.

D'Eramo, F., Pinotti, L., Tubía, J. M., Vegas, N., Aranguren, A. Tejero, R. & Gómez, D. 2006. Coalescence of lateral spreading magma ascending through dykes: a mechanism to form a granite canopy (El Hongo pluton, Sierras Pampeanas, Argentina). *Journal of the Geological Society, London* **163**, 881–92.

Dallmeyer, R. D. & Keppie, J. D. 1987. Polyphase late Paleozoic tectonothermal evolution of the southwestern Meguma Terrane, Nova Scotia: evidence from Ar^{40}/Ar^{39} mineral ages. *Canadian Journal of Earth Sciences* **24**, 1242–54.

Dehls, J. F., Cruden, A. R. & Vigneresse, J. L. 1998. Fracture Control of Late Archean Pluton Emplacement in the Northern Slave Province, Canada. *Journal of Structural Geology* **20** (9–10), 1145–54.

Djouadi, M. T., Gleizes, G., Ferré, E., Bouchez, J. L., Caby, R. & Lesquer, A. 1997. Oblique Magmatic Structures of Two Epizonal Granite Plutons, Hoggar, Algeria – Late-Orogenic Emplacement in a Transcurrent Orogen. *Tectonophysics* **279** (1–4), 351–74.

Gapais, D. 1989. Shear structures within deformed granites: mechanical and thermal indicators. *Geology* **17**, 1144–7.

Gebelin, A., Martelet, G., Chen, Y., Brunel, M. & Faure, M. 2006. Structure of late Variscan Millevaches leucogranite massif in the French Massif Central: AMS and gravity modelling results. *Journal of Structural Geology* **28** (1), 148–69.

Gleizes, G., Leblanc, D. & Bouchez, J.-L. 1997. Variscan granites of the Pyrenees revisited: their role as syntectonic markers of the orogen. *Terra Nova* **9**, 38–41.

Gleizes, G., Leblanc, D., Santana, V., Olivier, P. & Bouchez, J.-L. 1998. Sigmoidal Structures Featuring Dextral Shear During Emplacement of the Hercynian Granite Complex of Cauterets-Panticosa (Pyrenees). *Journal of Structural Geology* **20** (9–10), 1229–45.

Hill, J. D. 1988. Late Devonian peraluminous granitic plutons in the Canso area, eastern Meguma Terrane, Nova Scotia. *Maritime Sediments and Atlantic Geology* **24**, 11–19.

Hill, J. D. 1991. Petrology, tectonic setting, and economic potential of Devonian peraluminous granitoid plutons in the Canso and Forest Hills areas, eastern Meguma Terrane, Nova Scotia. *Geological Survey of Canada Bulletin* **383**. 96 pp.

Horne, R. & Culshaw, N. 2001. Flexural-slip folding in the Meguma Group, Nova Scotia. *Canada Journal of Structural Geology* **23** (10), 1631–52.

Housen, B. A., Richter, C. & van der Pluijm, B. A. 1993. Composite magnetic anisotropy fabrics: experiments, numerical models, and implications for the quantification of rock fabrics. *Tectonophysics* **220**, 1–12.

Hrouda, F. 1982. Magnetic anisotropy of rocks and its application in geology and geophysics. *Geophysical Surveys* **5**, 37–82.

Hrouda, F. 1993. Theoretical models of magnetic anisotropy to strain relationship revisited. *Physics of the Earth and Planetary Interiors* **77**, 237–49.

Ildefonse, B., Arbaret, L. & Diot, H. 1997. Rigid particles in simple shear flow: is their preferred orientation periodic or steady-state? *In* Bouchez, J.-L., Hutton, D. H. W. & Stephens, W. E. (eds) *Granite: from segregation of melt to emplacement fabrics*, 177–85. Dordrecht: Kluwer Academic Publishers.

Ishihara, S. 1981. The granitoid series and mineralization. *Economic Geology, 75th Anniversary Volume*, 458–84.

Jelinek, V. 1978. Statistical processing of anisotropy of magnetic susceptibility measured on groups of specimens. *Studia Geophyzika et Geodetika* **22**, 50–62.

Jelinek, V. 1981. Characterization of magnetic fabric of rocks. *Tectonophysics* **79**, 563–7.

Keppie, J. D. 1982. *Tectonic Map of the Province of Nova Scotia*. Nova Scotia, Halifax: Department of Mines and Energy.

Keppie, J. D. 1993. Synthesis of Palaeozoic deformational events and terrane accretion in the Canadian Appalachians. *Geologisches Rundschau* **82**, 381–431.

Keppie, J. D., Dallmeyer, R. D., Krogh, T. E. & Aftalion, A. 1993. Dating mineralization using several isotopic methods: and example from the South Mountain Batholith, Nova Scotia, Canada. *Chemical Geology* **103**, 251–70.

Keppie, J. D. & Dallmeyer, R. D. 1987. Dating transcurrent terrane accretion: an example from the Meguma and Avalon composite terranes in the northern Appalachians. *Tectonics* **6**, 831–47.

Kratinova, Z., Schulmann, K., Edel, J. B., Jezek, J. & Schaltegger, U. 2007. Model of successive granite sheet emplacement in transtensional setting: Integrated microstructural and anisotropy of magnetic susceptibility study. *Tectonics* **26** (6). doi:10.29/2006TC002035.

Leblanc, D., Gleizes, G., Roux, L. & Bouchez, J.-L. 1996. Variscan dextral transpression in the French Pyrenees: new data from the Pic des Trois-Seigneurs granodiorite and its country rocks. *Tectonophysics* **261**, 331–45.

March, A. 1931. Mathematische Theorie der Regelung nach der Korngestalt bei affiner Deformation. *Zeitschrift für Kristallographie* **81**, 285–97.

Mawer, C. K. & White, J. C. 1987. Sense of displacement on the Cobequid–Chedabucto fault system, Nova Scotia, Canada. *Canadian Journal of Earth Sciences* **24**, 217–23.

Mawer, C. K. & Williams, P. F. 1986. Structural study of highly deformed Meguma phyllite and granite, vicinity of White Head village, S.E. Nova Scotia. *Maritime Sediments and Atlantic Geology* **22**, 51–64.

Molyneux, S.J. & Hutton, D. H. W. 2000. Evidence for significant granite space creation by the ballooning mechanism: the example of the Ardara pluton, Ireland. *Geological Society of America Bulletin* **112**, 1543–58.

Muecke, G. K., Elias, P. & Reynolds, P. H. 1988. Hercynian/Alleghanian overprinting of an Acadian terrane. $^{40}Ar/^{39}Ar$ studies in the Meguma Zone, Nova Scotia, Canada. *Chemical Geology* **73**, 153–67.

Nadai, A. 1963. *Theory of flow and fracture of solids*, Volume 2. New York: McGraw-Hill. 705 pp.

Paterson, S. R., Vernon, R. H. & Tobisch, O. T. 1989. A review of criteria for the identification of magmatic and tectonic foliations in granitoids. *Journal of Structural Geology* **11**, 349–63.

Paterson, S. R., Fowler, T. K. Jr., Schmidt, K. L., Yoshinobu, A. S., Yuan, E. S. & Miller, R. B. 1998. Interpreting magmatic fabric patterns in plutons. *Lithos* **44**, 53–82.

Pignotta, G. S. & Benn, K. 1999. Magnetic fabric of the Barrington Passage pluton, Meguma Terrane, Nova Scotia: a two-stage fabric history of syntectonic emplacement. *Tectonophysics* **307** (1–2), 75–92.

Razanatseheno, M. O. M., Nédélec, A., Rakontondrazafy, M., Meert, J. G. & Ralison, B. 2010. Four-stage building of the Cambrian Carion pluton (Madagascar). *Earth and Environmental Science Transactions of the Royal Society of Edinburgh* **100**(for 2009), 133–45.

Reynolds, P. H., Zentilli, M. & Muecke, G. K. 1981. K–Ar and $^{40}Ar/^{39}Ar$ geochronology of granitoid rocks from southern Nova Scotia: Its bearing on the geological evolution of the Meguma Zone of the Appalachians. *Canadian Journal of Earth Sciences* **18**, 386–94.

Reynolds, P. H., Elias, P., Muecke, G. K. & Grist, A. M. 1987. Thermal history of the southwestern Meguma zone, Nova Scotia, from an $^{40}Ar/^{39}Ar$ and fission track dating of intrusive rocks. *Canadian Journal of Earth Sciences* **24**, 1952–65.

Richter, C. 1992. Particle motion and the modelling of strain response in magnetic fabrics. *Geophysical Journal International* **110**, 451–64.

Rochette, P. 1987. Magnetic susceptibility of the rock matrix related to magnetic fabric studies. *Journal of Structural Geology* **9**, 1015–20.

Rochette, P., Jackson, M. & Aubourg, C. 1992. Rock magnetism and the interpretation of anisotropy of magnetic susceptibility. *Reviews of Geophysics,* **30**, 209–26.

Rochette, P., Aubourg, C. & Perrin, M. 1999. Is this magnetic fabric normal? A review and case studies in volcanic formations. *Tectonophysics* **307** (1–2), 219–34.

Sanderson, D. J. & Marchini, W. R. D. 1984. Transpression. *Journal of Structural Geology* **6**, 449–58.

Schenk, P. E. 1971. Southeastern Atlantic Canada, northwestern Africa, and continental drift. *Canadian Journal of Earth Sciences* **8**, 1218–35.

Schenk, P. E. 1995. Meguma Zone. *In* Williams, H. (ed.) *Geology of the Appalachian–Caledonian Orogen in Canada and Greenland. Geology of Canada*, 261–77. Ottawa: Geological Survey of Canada.

Siegesmund, S. & Becker, J. K. 2000. Emplacement of the Ardara pluton (Ireland): new constraints from magnetic fabrics, rock fabrics and age dating. *International Journal of Earth Sciences* **89**, 307–27.

Tate, M. C., Clarke, D. B. & Heaman, L. M. 1997. Progressive hybridisation between Late Devonian mafic-intermediate and felsic magmas in the Meguma Zone of Nova Scotia, Canada. *Contributions to Mineralogy and Petrology* **126**, 401–15.

Tikoff, B. & Teyssier, C. 1994. Strain modeling of displacement-field partitioning in transpressional orogens. *Journal of Structural Geology* **16**, 1575–88.

Tobisch, O. T. & Cruden, A. R. 1995. Fracture-controlled magma conduits in an obliquely convergent continental magmatic arc. *Geology* **23**, 941–4.

Urai, J. L., Means, W. D. & Lister, G. S. 1986. Dynamic recrystallization of minerals. *In* Hobbs, B. E. & Heard, H. C. (eds) *Mineral and Rock Deformation: Laboratory Studies. Geophysical Monograph*, 161–99. Washington: American Geophysical Union.

Vernon, R. H. 2000. Review of microstructural evidence of magmatic and solid-state flow. *Electronic Geosciences* **5** (2): http://link.springer-ny.com/link/service/journals/10069/bibs/0005001/00050002.htm.

Vigneresse, J.-L. & Bouchez, J.-L. 1997. Successive Granitic Magma Batches During Pluton Emplacement – the Case of Cabeza De Araya (Spain). *Journal of Petrology,* **38** (12), 1767–76.

Williams, H. & Hatcher, R. H. J. 1982. Suspect terranes and accretionary history of the Appalachian orogen. *Geology* **10**, 530–6.

Žák, J., Schulmann, K. & Hrouda, F. 2005. Multiple magmatic fabrics in the Sazava pluton (Bohemian Massif, Czech Republic): a result of superposition of wrench-dominated regional transpression on final emplacement. *Journal of Structural Geology* **27** (5), 805–22.

MS received 29 January 20008. Accepted for publication 30 April 2008 (Stellenbosch); 15 January 2009 (RSE).